ADVANCED ENERGY MATERIALS
www.advenergymat.de

Enhanced Near-Bandgap Response in InP Nanopillar Solar Cells

*Corsin Battaglia, Jingsan Xu, Maxwell Zheng, Xingtian Yin, Mark Hettick, Kevin Chen, Nancy Haegel, and Ali Javey**

The effect of nanopillar texturing on the performance of InP solar cells is investigated. Maskless, lithography-free reactive ion etching of InP nanopillars improves the open-circuit voltage, reduces reflectance over a broad spectral range, and enhances the near-bandgap response compared to a flat, non-textured cell with comparable reflectance in the infrared. Electron-beam induced current measurements indicate an increased effective minority carrier collection length. The response at short wavelengths decreases due to the formation of a defective surface layer with strong non-radiative recombination. Plasma oxidation and wet etching partially restore the blue response resulting in a power conversion efficiency of 14.4%.

1. Introduction

Nanopillar solar cells have attracted much attention with the promise of enhanced performance at lower cost. Compared to planar cell architectures, nanopillars can enhance light absorption and improve carrier collection, thereby requiring less material and tolerating lower material quality.[1–6] However, increased non-radiative surface recombination associated with their large surface area often compensates performance gains and explains why, as of today, nanopillar solar cells have not yet been able to outperform their planar counterparts.[7]

In contrast to other III-V semiconductors, untreated InP possesses a relatively low surface recombination velocity,[8] which makes it an ideal material system for large surface-area nanopillar devices. InP nanopillars were recently shown to improve the performance of photocathodes for solar hydrogen production.[9] Compared to a planar reference, the implementation of nanopillars improved both photocurrent and onset potential, but the exact mechanism for this improvement remained unclear.

Here we investigate the effect of nanopillar texturing on the performance of InP solar cells. On the optical level, nanopillars minimize the reflectance over a broad spectral range. Mapping the current generated by an electron beam across the cell cross-section, we further show that texturing increases the effective minority carrier collection length leading to improved photocurrent and open-circuit voltage and a power conversion efficiency of 14.4%.

2. Results and Discussion

Nanopillars are fabricated via maskless, lithography-free reactive ion etching (RIE). The entire device fabrication avoids the use of expensive metal-organic precursor gases necessary for the fabrication of III-V solar cells via traditional chemical vapor deposition. In addition, we recently introduced a thin-film vapor-liquid-solid growth technique for the growth of high-quality InP thin films (1–3 μm) on cheap non-epitaxial substrates,[10] enabling future elimination of the thick (350 μm) expensive InP wafers used in this work which, together with the precursor gases, represent the dominant cost drivers for III-V photovoltaics.[11]

A sketch of the fabrication flow is shown in **Figure 1**a. Zn-doped p-type InP wafers with a carrier density of 3×10^{17} cm^{-3} are etched in hydrochloric (HCl) acid (6%) for 30 s to remove the native oxide. An ohmic backcontact is formed by sputtering a thin layer of Zn (20 nm) capped with a Au layer (100 nm) and subsequent annealing at 420 °C in forming gas (H_2:N_2 = 5%) for 45 min. The front side is wet etched again in HCl (6%) and dry etched in a H_2:CH_4:Ar plasma (40 sccm: 10 sccm: 10 sccm) at a pressure of 110 mTorr, a power density of 0.5 W cm^{-2} and a bias voltage of 500–550 V to form the nanopillars. Following oxidation in a O_2 plasma[12] and etching in HCl (3%) for 30 s to remove undesired metallic indium residues and the defective InP layer (see discussion below) formed during the RIE process at the pillar surface, a conformal transparent conductive indium tin oxide electrode (ITO, In_2O_3:SnO = 90%:10%, 35 nm) is deposited by RF sputtering at room temperature at

Dr. C. Battaglia, Dr. J. Xu, M. Zheng, X. Yin, M. Hettick, K. Chen, Prof. A. Javey
Electrical Engineering and Computer Sciences Department
University of California Berkeley
Berkeley, CA 94720, USA
E-mail: ajavey@eecs.berkeley.edu
Dr. C. Battaglia, Dr. J. Xu, M. Zheng, X. Yin, M. Hettick, K. Chen, Prof. A. Javey
Materials Sciences Division
Lawrence Berkeley National Laboratory
Berkeley, CA 94720, USA
N. Haegel
Physics Department
Naval Postgraduate School
Monterey, CA 93943, USA

DOI: 10.1002/aenm.201400061

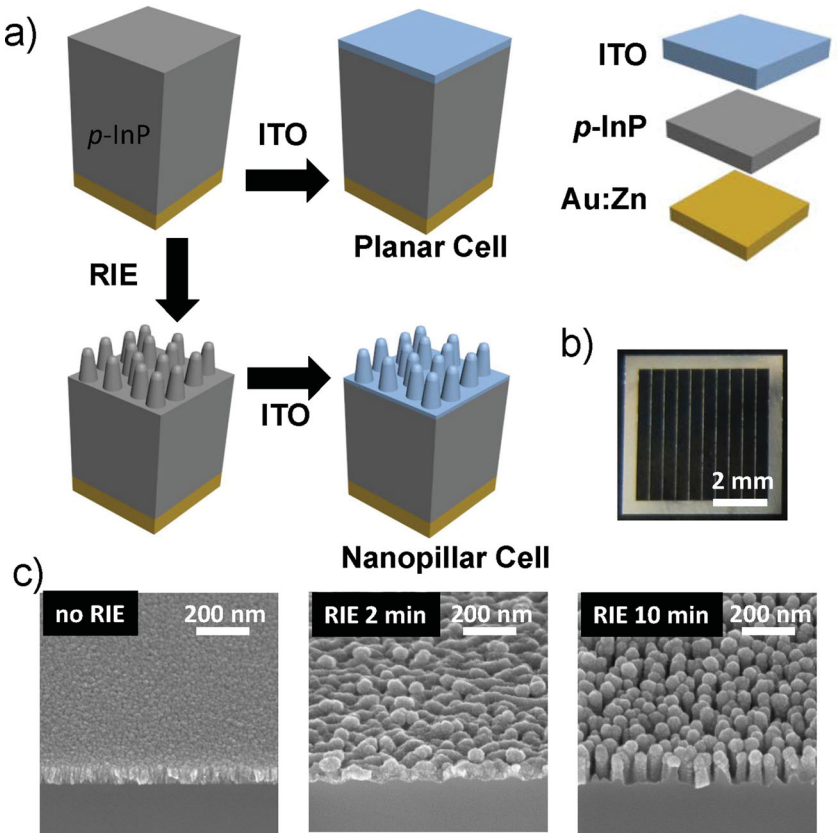

Figure 1. a) Schematics of the InP solar cell fabrication process for both nanopillar and planar geometries. b) Photograph of a fabricated cell with Ag finger grid. c) Cross-sectional SEM images of of the fabricated InP nanopillar solar cells after ITO deposition as a function of RIE time (0, 2 and 10 min).

7 mTorr in Ar gas. Note that similar surface oxidation/etching concepts have been applied previously to other material systems, including Si nanopillars with a similar goal of improving surface properties.[13] For comparison, a flat, non-textured reference device was fabricated by omitting the dry etching step and using a thicker ITO layer (70 nm) such that the reflectance minimum, caused by destructive interference of incoming and reflected light, falls into the center of the visible region of the spectrum, resulting in maximum light in-coupling into the InP absorber. Photolithography and lift-off were used to mask and pattern the cells into 5×5 mm^2 areas with evaporated 100 nm thick Ag grid with finger width and pitch of 11 µm and 490 µm (Figure 1b). Cells were characterized under simulated 1-sun illumination (1000 W m^{-2}, global air mass 1.5 spectrum, 25 °C).

Figure 1c shows scanning electron microscopy (SEM) images of the front surface of the final solar cells as a function of RIE time. During RIE, InP is reduced in the hydrogen-rich plasma and phosphorus leaves the surface. The remaining indium agglomerates into small indium droplets at the surface[14] which leads to self-masking during etching and consequently to the formation of InP nanopillars with a characteristic diameter on the order of 50 nm and increasing height which reaches ≈125 nm after 10 min etching as can be seen from Figure 1c.

While RIE is usually detrimental for the electrical performance of a photovoltaic absorber layer,[15] we observe that nanotexturing leads to an improvement in open-circuit voltage (V_{oc}) as seen in the current-voltage (J–V) characteristics measured under 1-sun in **Figure 2**a. The V_{oc} increases from the initial 615 mV to 740 mV after 2 min RIE and saturates at 770 mV for etching times equal or longer than 10 min. The short-circuit current density (J_{sc}) and fill factor (FF) also improve. Cell performance parameters are summarized in **Table 1**. The highest power conversion efficiency is obtained after 10 min RIE reaching 14.4%.

In the past, ion bombardement during ITO sputtering on flat InP was suggested to cause defect-induced type conversion of the near surface region from p-type to n-type resulting in a buried homojunction.[16] This has been confirmed in a series of experiments summarized in ref. [17]. Passivation of zinc acceptors was ruled out as the main cause for type conversion. Instead the formation of phosphorus vacancies was identified as the dominant mechanism leading to type conversion.[18] Type conversion is also expected to be the main reason for the enhanced junction properties in RIE treated cells. In fact, InP possesses a strong tendency to convert to n-type when the native defect density is sufficiently high, as the Fermi level stabilizes at an energy closer to the conduction band minimum than the valence band maximum.[19] This leads to the formation of a buried graded InP n-p homojunction which improves

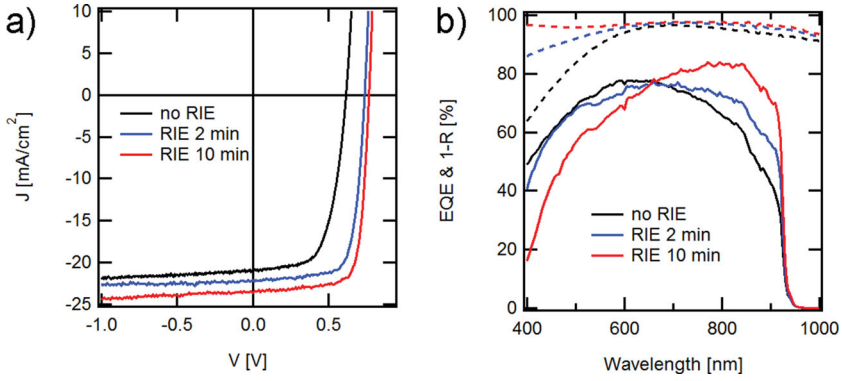

Figure 2. a) J–V characteristics under 1-sun illumination of InP nanopillar solar cells fabricated with different RIE texturing times (2 and 10 min). The data for a planar reference cell (i.e., without RIE texturing) is also shown. b) EQE (solid lines) and 1–R (dashed lines) plots as a function of wavelength for planar and RIE textured InP cells, corresponding to the devices shown in panel (a).

Table 1. Performance characteristics of InP nanopillar solar cells.

Etching time [min]	V_{oc} [mV]	J_{sc} [mA cm^{-2}]	FF [%]	Eff [%]
0	615	20.9	53	6.8
2	740	22.1	76	12.4
10	770	23.6	79	14.4

the V_{oc}. In addition, the high n-type conductivity of InP in the near surface region contributes to the improvement in FF even at reduced ITO thickness. Defect induced stabilization of the Fermi energy has been explained within the amphoteric defect model.[20]

Inspection of the external quantum efficiency (EQE) shown in Figure 2b reveals a strong enhancement in the near-bandgap response after 10 min RIE accounting for 2.6 mA cm^{-2} additional photocurrent for wavelengths longer than 700 nm. Importantly the reflectance (R) of the textured cell (shown as 1–R in Figure 2b) for wavelengths longer than 700 nm is very similar to the flat cell owing to the proper thickness of the ITO layer. Thus the current enhancement cannot be attributed to a change of light in-coupling into the absorber, but must stem from a modification of the generation or collection profile in the absorber itself (see detailed discussion below).

From Figure 2b, we further see that the short wavelength response below 700 nm is strongly attenuated resulting in a reduction of photocurrent by 2.4 mA cm^{-2}. This reduction occurs despite the fact that the nanopillars provide much superior antireflection than the interference-based and wavelength-dependent antireflection of the flat cell, as can be seen from the reflectance measurements also shown in Figure 2b. The reduction in the short wavelength response can be explained with the formation of a highly defective "dead" layer at the InP surface in which photogenerated minority carriers recombine non-radiatively before being collected.

Figure 3a shows the EQE of a cell, for which the O_2 plasma oxidation step and HCl etch treatment, which serves to remove at least partially the dead layer after the RIE process, was omitted. The spectral response is strongly attenuated from 400 nm all the way up to 900 nm resulting in a marked short-circuit current loss of 6.1 mA cm^{-2} compared to the textured cell fabricated with the dead layer removal step. However, repeating the O_2 plasma oxidation and HCl etch step to thin the dead layer further leads to only marginal further improvements in short-circuit current (0.2 mA cm^{-2} after 3 cycles) because of a simultaneous increase in cell reflectance resulting from the flattening of the nanopillar texture. Furthermore the open-circuit voltage starts to drop (30 mV after three cycles) resulting in a decrease of the overall power conversion efficiency.

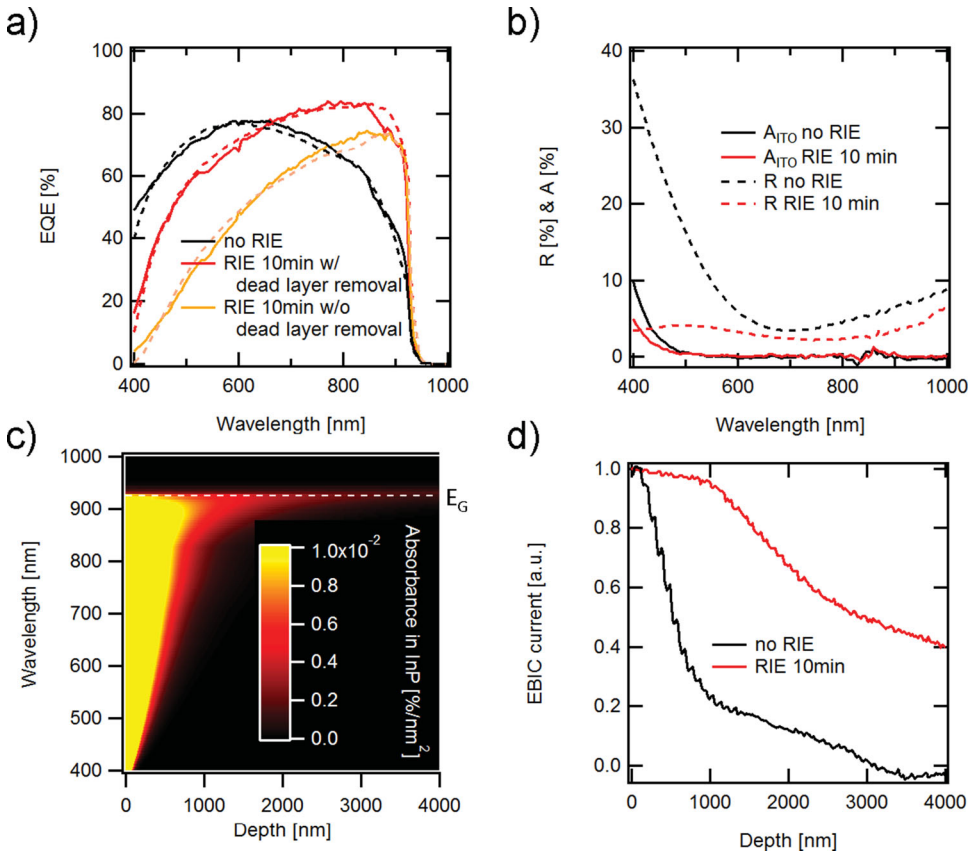

Figure 3. a) Effect of dead layer removal on EQE. Experimental measurements are shown as continuous lines, and modeled profiles are shown as dashed lines. b) Reflectance of the cells and absorbance of the ITO layer for planar and RIE textured (10 min) samples. c) The calculated optical generation profile of InP cells determined from the InP absorption coefficient, and by taking into account cell reflectance and ITO absorbance. d) Cross-sectional EBIC profiles as a function of beam excitation position for planar and RIE textured (10 min) InP cells.

To better understand the origins of the enhanced near-bandgap response, we model the EQEs at each wavelength λ by EQE = $(1 - R)(1 - A_{ITO})\int dz[(1 - \exp(-\alpha_{InP}z))\eta_{col}(z)]$. The integral is performed over the depth z. R is the reflectance of the cell (dashed lines in Figure 3b) measured with a photospectrometer. A_{ITO} is the absorbance of the ITO layer (continuous lines in Figure 3b) determined by measuring transmittance T and reflectance R of ITO on a glass slide and calculating $A = 1 - T/(1 - R)$. α_{InP} is the experimental absorption coefficient of InP taken from literature.[21] The product $(1 - R)(1 - A_{ITO})(1 - \exp(-\alpha_{InP}z))$ represents the z- and λ-resolved optical generation profile in InP shown in Figure 3c. $\eta_{col}(z)$ represents the depth-dependent collection probability of excited minority carriers, which we obtain from electron-beam induced current (EBIC) traces shown in Figure 3d measured at 10 keV for a cleaved device in cross-section. Similar profiles were obtrained over a range of probe currents in the low excitation limit. During EBIC measurements, impinging electrons generate minority carriers which are then extracted through the junction and measured as a current. As minority carrier generation by an electron beam is local, EBIC allows to map the spatially resolved collection probability which is proportional to the measured current. From Figure 3d it can be seen that the EBIC signal, and consequently the collection probability, away from the surface increases strongly after RIE. This is consistent with the enhanced red response in the EQE as electron-hole pairs generated by long wavelength photons are generated deeper inside the bulk as can be seen from Figure 3c. The characteristic decay lengths obtained by extracting the inverse slopes of a linear fit to the initial linear range of the EBIC signal in Figure 3d in a semi-logarithmic plot are 0.5 µm and 2.6 µm for the sample without and with reactive ion etching respectively. For the ideal case of an abrupt junction, the collection probability $\eta_{col} = 1$ in the depletion region with width W decays exponentially in the quasi-neutral region $\eta_{col} = \exp(-(z - W)/L_d)$ with a characteristic decay length corresponding to the minority carrier diffusion length L_d, which is commonly extracted from EBIC traces. In contrast, RIE is expected to result in a graded junction such that the extracted value represents an improved effective collection length, which explains the enhanced red response and improved FF. In addition, we also expect that recombination of carriers due to the proximity of the cross-sectional surface will affect the absolute magnitude of the collected current signature. The EBIC signal will show, however, the spatial variation of the collection efficiency for a fixed carrier generation depth.

In order to take the dead layer at the InP surface into account in our model we set $\eta_{col} = 0$ for $0 \le z \le d_{dead}$, where d_{dead} is the dead layer thickness. d_{dead} respresents the only adjustable parameter in our model. All other values are taken from experiment. The simulated EQE curves (dashed lines) are shown in Figure 3a along with the experimental EQE curves (continuous lines) discussed before. Although our simple model neglects nanophotonic and electrical effects due to the nanopillar morphology and treats the dead layer as an absorbing flat slab of thickness d_{dead}, the correspondence between model and experiment is excellent. From our model we extract dead layer thicknesses of 40 nm and 90 nm for the 2 min and 10 min etched samples respectively. This estimation roughly agrees with the maximum penetration depth of hydrogen atoms with a kinetic energy of 500–550 V (equal to the plasma bias) into flat InP determined to be 50 nm by Monte Carlo simulations.[22] The maximum penetration depth for carbon and argon atoms is only of the order of 10 nm, but argon is heavy enough to lead to sputtering. The dead layer thicknesses are below the resolution limit of EBIC, which is given by the size of the interaction volume of the electron beam with InP and is approximately ≤1 µm for 1 keV electrons on InP.

Although nanopillar structures are often introduced into solar cells with the expectation of enhancing light absorption through nanophotonic light scattering, our modeling results show that such effects only play a secondary role here. In fact, incoming short wavelength light is expected to be scattered into shallower angles in the nanostructured case as compared to the planar case. However due to the dead layer, this effect is completely masked. For long wavelength light, the nanopillars can be assumed to act as an effective medium, with a mean refractive index weighted by the corresponding volumes of InP, ITO and air. Consequently scattering is only minimal and does not contribute significantly to enhance light absorption within the collection length. However, the nanopillars prove to be an excellent broad band antireflective layer maximizing light incoupling into InP.

It remains surprising that RIE improves carrier collection far beyond the penetration depth of hydrogen species into InP, as evidenced by both the spectral dependence of the EQE and the cross-sectional EBIC. A similar phenomenon was also observed for other III-V materials.[23] Channeling was excluded as a sufficient explanation as it can increase the penetration depth of atoms by a factor of ≈8 only. It is well known that the presence of hydrogen accelerates the decomposition of InP through the depletion of phosphorus.[24] This can be thought of as a generation source for phosphorus vacancies at the surface, which then diffuse into the bulk due to the creation of a strong chemical potential gradient. In addition, an electric field builds up in the depletion region due to the type conversion of the near-surface region. This can result in an additional drift component of positively charged phosphorus vacancies, which drives them into the bulk. Note that within the amphoteric defect model, the effective charge state of native defects, such as phosphorus vacancies, also depends on the position of the Fermi level with respect to the Fermi stabilization energy. In p-type InP, this would suggest native defects act as donors.

An alternative to improve the red response in flat ITO/InP solar cells was demonstrated in ref. [25] by reducing the carrier concentration in the InP wafer. **Figure 4** compares EQE measurements for InP cells with ionized bulk acceptor concentrations of 3×10^{17} cm^{-3} as for all previous cells and a lower concentration of 3×10^{16} cm^{-3}. The short-circuit current for the flat and nanopillar textured cell improves by 1.2 mA cm^{-2} and 1.6 mA cm^{-2} respectively. For both cells the enhancement happens over the full spectral range. However in both cases the fill factor drops due to the higher series resistance of the bulk wafer in agreement with ref. [25] compensating the improved current.

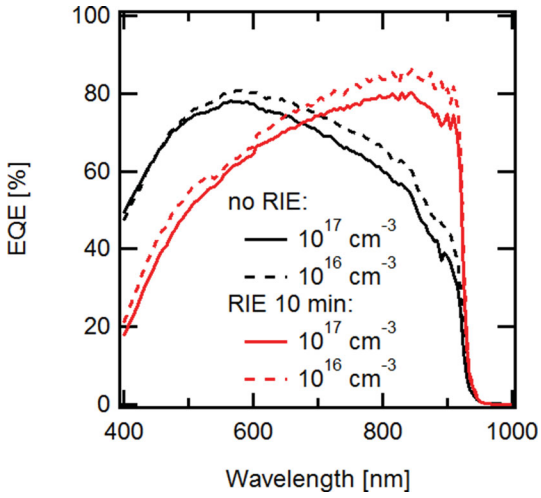

Figure 4. EQE spectra of flat and RIE textured (10 min) InP solar cells for two different body doping concentrations (10^{16} and 10^{17} cm^{-3}).

3. Conclusion

In conclusion, we have fabricated InP nanopillar solar cells with a power conversion efficiency of up to 14.4%. Nanopillars minimize the cell reflectance over a broad spectral range. The enhanced near-bandgap response is well explained by EBIC results showing improved carrier collection from the bulk consistent with the formation of a graded buried junction during RIE. Cell efficiencies can be improved further by reducing/avoiding the formation of a dead layer, while maintaining a high open-circuit voltage. In the future, the nanopillar fabrication and device architecture reported here will be applied to boost the performance of thin InP films (1–3 µm) grown by the thin-film vapor-liquid solid growth technique introduced recently.[10]

Acknowledgements

C.B. and J.X. contributed equally to this work. InP solar cell fabrication and characterization was funded by the Bay Area Photovoltaics Consortium (BAPVC). C.B. acknowledges support from the Zeno Karl Schindler Foundation.

Received: January 12, 2014
Revised: February 14, 2014
Published online:

[1] J. Oh, H.-C. Yuan, H. Branz, *Nat. Nanotechnol.* **2012**, *7*, 743.
[2] M. D. Kelzenberg, D. B. Turner-Evans, M. C. Putnam, S. W. Boettcher, R. M. Briggs, J. Y. Baek, N. S. Lewis, H. A. Atwater, *Energy Environ. Sci.* **2011**, *4*, 866.
[3] J. Wallentin, N. Anttu, D. Asoli, M. Huffman, I. Abert, M. H. Magnusson, G Siefer, P. Fuss-Kailuweit, F. Dimroth, B. Witzigmann, Q. Xu, H. L. Samuelson, K. Deppert, M. T. Borgström, *Science* **2013**, *339*, 1057.
[4] Z. Fan, H. Razavi, J.-W. Do, A. Moriwaki, O. Ergen, Y.-L. Chueh, P. W. Leu, J. C. Ho, T. Takahashi, L. A. Reichertz, S. Neale, K. Yu, M. Wu, J. W. Ager, A. Javey, *Nat. Mater.* **2009**, *8*, 648.
[5] D. Liang, Y. Kang, Y. Huo, Y. Chen, Y. Cui, J. Harris, *Nano Lett.* **2013**, *13*, 4850.
[6] R. Kapadia, Z. Fan, K. Takei, A. Javey, *Nano Energy* **2012**, *1*, 132.
[7] M. A. Green, K. Emery, Y. Hishikawa, W. Warta, E. D. Dunlop, *Prog. Photovolt: Res. Appl.* **2013**, *21*, 827.
[8] Y. Rosenwaks, Y. Shapira, D. Huppert, *Phys. Rev. B* **1991**, *44*, 13097.
[9] M. H. Lee, K. Takei, J. Zhang, R. Kapadia, M. Zheng, Y.-Z. Chen, J. Nah, T. S. Matthews, Y.-L. Chueh, J. W. Ager, A. Javey, *Angew. Chem. Int. Ed.* **2012**, *51*, 10760.
[10] R. Kapadia, Z. Yu, H.-H. H. Wang, M. Zheng, C. Battaglia, M. Hettick, D. Kiriya, K. Takei, P. Lobaccaro, J. W. Beeman, J. W. Ager, R. Maboudian, D. C. Chrzan, A. Javey, *Sci. Rep.* **2013**, *3*, 2275.
[11] M. Woodhouse, A. Goodrich, R. Margolis, T. L. James, M. Lokane, R. Eggert, *IEEE J. Photovolt.* **2013**, *3*, 833.
[12] D. T. Clark, T. Fok, *Thin Solid Films* **1989**, *78*, 271.
[13] H.-P. Wang, T.-Y. Lin, C.-W. Hsu, M.-L. Tsai, C.-H. Huang, W.-R. Wei, M.-Y. Huang, Y.-J. Chien, P.-C. Yang, C.-W. Liu, L.-J. Chou, J.-H. He, *ACS Nano* **2013**, *7*, 9325.
[14] S. J. Pearton, U. K. Chakrabarti, A. P. Perley, *J. Appl. Phys.* **1990**, *68*, 2760.
[15] W. A. Nositschka, O. Voigt, P. Manshande, H. Kurz, *Sol. Energy Mater. Sol. Cells* **2003**, *80*, 227.
[16] M.-J. Tsai, A. L. Fahrenbruch, R. H. Bube, *J. Appl. Phys.* **1980**, *51*, 2696.
[17] T. J. Coutts, M. W. Wanlass, T. A. Gessert, X. Li, J. S. Ward, Third International Conference on Indium Phosphide and Related Materials, IEEE, Cardiff, **1991**, p. 20, http://dx.doi.org/10.1109/ICIPRM.1991.147286
[18] X. Li, T. A. Gessert, T. J. Coutts, *AIP Conf. Proc.* **1991**, *227*, 126.
[19] W. Walukiewicz, *Physica B* **2001**, *302–303*, 123.
[20] W. Walukiewicz, *J. Vac. Sci. Technol. B* **1987**, *5*, 1062.
[21] E. D. Palik, *Handbook of Optical Constants and Solids*, Online version, Elsevier, Amsterdam, 1997.
[22] J. F. Ziegler; SRIM-2003, *Nuclear Instruments and Methods in Physics Research Section B: Beam Interactions with Materials and Atoms* **2004**, *219–220*, 1027.
[23] S. J. Pearton, *Int. J. Mod. Phys. B* **1994**, *14*, 1781.
[24] T. Sugino, H. Yamamoto, J. Shirafuji, *Jpn. J. Appl. Phys.* **1991**, *30*, L948.
[25] T. J. Coutts, S. Naseem, *Appl. Phys. Lett.* **1985**, *46*, 164.